JOURNAL OF CATALYSIS 7, 191–197 (1967)

Diffusional Mass Transport of Nonadsorbed Gases within Porous Structures

II. Structural Significance of the Convergent–Divergent Pore Model

RICHARD N. FOSTER,* JOHN B. BUTT, AND HARDING BLISS

From the Department of Engineering and Applied Science, Yale University, New Haven, Connecticut

Received August 24, 1966; revised October 24, 1966

Experimental results of counterdiffusion studies are correlated with the convergent–divergent pore structure model proposed previously. Relationship of the parameters of the model to porous structure properties is discussed; it is shown that these quantities may be determined from the volume–area distribution of a material and that the model may thus be employed for prediction of porous structure effects on diffusional mass transport.

In previous work with the convergent–divergent pore model (*1*), we have been especially concerned with demonstrating that porosity and other overall properties of porous structures are dependent on the distribution of volume and area within the material and that any computational representation of the structure should accordingly be dependent on this distribution. The correlation of flux data with the computational model also requires a value for the mixing parameter (the "efficiency"), which is based on a total length agreement between the segments of the two arrays required for mixing to occur. Also, the convention of reporting experimental flux measurements on the basis of total exposed pellet area in the Wicke-Kallenbach cell rather than actual void area requires assignment of a value for this area, since the flux employed in Eq. (2) of Part I (preceding paper) must be based on actual rather than effective area. Thus, it is necessary to introduce the concept of macropore surface porosity, the fraction of actual surface area occupied by pores. Changing the value of the mixing efficiency serves to shift the computed flux–pressure curve either up or down but does not alter the shape of the curve, which is entirely determined by the pore-size distribution and the macropore surface porosity.

The values of computed flux, then, depend on values of the mixing efficiency and surface porosity. It will be shown subsequently that mixing efficiency can be predicted from overall properties of the porous structure, and that the value for surface porosity employed in the computations can be reconciled with those computed theoretically for some limiting types of structure. For the present, however, it will suffice to regard these as parameters whose values are assigned on the basis of the best fit between experimental and computed flux–pressure–temperature data.

Comparison of Predicted and Measured Fluxes

In Figs. 5 to 9 and 11 of Part I are presented the curves computed from the convergent–divergent pore model, together with the experimental data, for the supported nickel oxide and molybdena pellets. Variation of flux with pressure, temperature, and porosity (for the molybdena)

* Present address: Union Carbide International Co., New York, N. Y.

are correlated in these computations. The computed values reported are those determined for best fit to the argon flux data. Helium flux values are determined from the argon values and the theoretical flux ratio of 3.16. Better fits on flux–pressure at high pressure could probably have been obtained if helium flux had been used as a basis for the correlation (deviations from experimental would then be divided by 3.16 in obtaining the argon curve, rather than being multiplied by that factor as in the present case), or if both sets of data had been used. The calculations reported here are seen to fit the data quite well, however; the initial slopes of the calculated flux–pressure curves appear somewhat greater than those of the data but the difference is small. The temperature dependence of diffusional flux, including the inversion phenomena, is well correlated by the model, as shown in Fig. 9 of Part I. Variation of flux with porosity as predicted by the model also agrees well with experimental data. For porous structures of similar volume–area distribution such as the molybdena there seems to be a correlation of flux and porosity which is almost linear over small ranges of porosity; the porosity–flux relationship is sensitive to the volume–area distribution, though, as demonstrated in the present work by the results for the nickel oxide pellet (of almost the same porosity as molybdena pellet 4) which do not fit the experimental trends of the molybdena. It is worthy of note that the convergent–divergent pore model calculation correlates flux data for both types of structures.

A comparison of the results of computation by the convergent-divergent pore model with those of the recently postulated "random pore" model of Wakao and Smith (*2*) for some of the porous solids of this study is given in Fig. 1. It is seen that the calculated flux–pressure relationship for the nickel oxide pellet has approximately the same shape as the experimental data; however the predicted values of Wakao and Smith are about 30% too low. The molybdena pellet offers a more striking example. In this case the slope of the Wakao and Smith prediction is much smaller than that of the observed data and the calculation of the convergent–divergent model. Further, the values of the flux from the random pore prediction fall almost an order of magnitude below the data. It is felt that the failure of the random pore model in the cases illustrated is primarily the result of an oversimplified

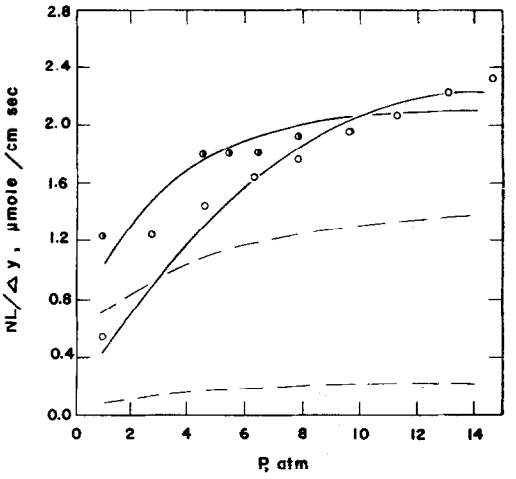

FIG. 1. Comparison of convergent–divergent and random pore model predictions of flux-pressure relationship for nickel and molybdena samples. Open points represent argon flux data for supported nickel oxide sample, half-closed points for molybdena sample 2 at 0°C. Solid lines computed from convergent–divergent pore model, dashed lines from random pore model.

approach which postulates flux to be proportional to the square of volume porosity and capillary dimension as defined from average pore radius. While the method will undoubtedly have application to interpretation of transport in structures of similar type, and is of particular utility because of its simplicity, it does not appear able to account for wide variations in pore structure as characterized by differing pore volume–area distributions.

The agreement between experimental and computed values reported here indicates that the convergent–divergent pore model offers excellent correlation of the observed phenomena. There are two important factors yet to be discussed, though, which have considerable bearing on whether the

model can assume perdictive, as distinct from correlative, functions. The first of these is the relationship between surface and volume porosities, and the second is the mixing parameter.

Effect of Surface Porosity

The surface porosity, that is the void area in a plane perpendicular to the direction of diffusional transport, is taken to be ⅔ of the volume porosity in the pore model, as described elsewhere (*1*). This factor then appears directly in the flux values employed for the iterative computation using Eq. (2) of Part I and the computed results reported here incorporate this assumption. It is possible to derive a relationship between surface porosity and volume porosity if some type of specific structure is employed to specify the porous material. This is not the same as describing pore shapes, since the structure of the porous material describes its geometrical properties while the description of pore shapes attempts to define individual factors which account for the transport resistances within the medium.

Two limiting types of structures will be discussed, the block structure of Fig. 2, bottom and the Emmenthal structure of Fig. 2, top. The block structure pictures the porous medium as a collection of uniformly sized cubic powder particles, with the pore being formed by the interstitial spaces between the particles. The Emmenthal structure describes the porous medium as a collection of mutually orthogonal rectangular pores embedded in a solid block. The void volume of the block model is given by

$$V_{\text{voids}} = 3nxa^2 - 3n^2x^2a + n^3x^3 \quad (1)$$

in which n is the number of pores on a side, x the width of a pore, and a the length of both pore and particle. The first term on the right-hand side of Eq. (1) represents the volume of a slab through the porous particle whose area is a^2 and whose thickness is x. There will be n of these slabs oriented in each of three mutually orthogonal directions so total volume is $3nxa^2$. This volume is an approximation to the void volume; however the volume common to a pair of slabs is counted twice. This volume is given by the second term, consisting of a collection of rectangular voids oriented in each direction. The adjustment of the second term is too large, however, since it has not accounted for the volume of three mutually

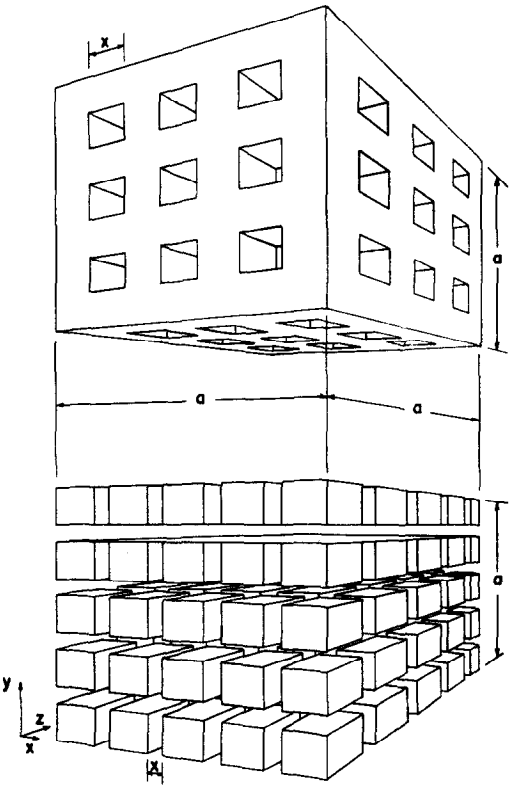

Fig. 2. Idealized structure types: top, Emmenthal structure; bottom, block structure.

perpendicular voids which occur at the intersection of three mutually orthogonal void slabs. The volume of the intersections of these voids is x^3 and there will be n^3 intersections in the porous material. The total volume of these intersections is n^3x^3, as given in the final additive term of Eq. (1). Total volume of the unit of material is a^3, thus the volume porosity of this model is given by

$$\epsilon_v = 3\mu - 3\mu^2 + \mu^3 \quad (2)$$

where μ may be regarded as a type of linear porosity and is defined as nx/a. The

void area, A_s, perpendicular to the direction of net transport at any point within the volume is now easily computed as

$$A_s = 2nxa - n^2x^2 \quad (3)$$

The first term gives the area of all the rectangular strips x wide and a long. The area of the intersections of these strips has been counted twice so the amount n^2x^2 must be subtracted in order to obtain the correct result. By defining surface porosity, ϵ_s, as the ratio of A_s to the total area of the normal face, it is found that

$$\epsilon_s = 2\mu - \mu^2 \quad (4)$$

The relationship between the surface porosity and the volume porosity for the block structure is then given by

$$(\epsilon_s/\epsilon_v) = (2 - \mu)/[3(1 - \mu) + \mu^2] \quad (5)$$

in which $0 \leqslant \mu \leqslant 1$. There also exists a simple relationship between μ and ϵ_v, namely

$$\mu = 1 - (1 - \epsilon_v)^{1/3} \quad (6)$$

and the combination of Eqs. (5) and (6) provides the desired relationship between (ϵ_s/ϵ_v) and ϵ_v, which is the experimentally determined quantity.

Equations of the same sort can be derived for the Emmenthal structure. They are

$$\epsilon_v = 3\mu^2 - 3\mu^3 \quad (7)$$

and

$$(\epsilon_s/\epsilon_v) = 1/(3 - 2\mu) \quad (8)$$

The relationships of Eq. (5) to Eq. (8) are given in Fig. 3. The results for $(\epsilon_s/\epsilon_v) = f(\epsilon_v)$ are presented for both structures in Fig. 4.

The differences between the block and Emmenthal structures are apparent in Fig. 4. The curves represent limiting conditions for the relationship between the surface and volume porosity. It is not unreasonable to assume that real porous particles probably vary somewhere between these limits. The dashed line in Fig. 4 is an average between the two structures, determined by averaging the plots of Fig. 3 and plotting the resulting relationship between (ϵ_s/ϵ_v) and ϵ_v. It is seen that the surface porosity would normally be expected to vary between practical limits of roughly 0.50 and 0.65 for the range of ϵ_v (~0.15 to 0.5) corresponding to porous structures of this sort reported in the literature. Although the value of 0.67 used in correlation of data, chosen initially on an intuitive basis, is somewhat higher than the indicated range it is still well within the range of feasible values. [For a thorough discussion of such models, see ref. (3).]

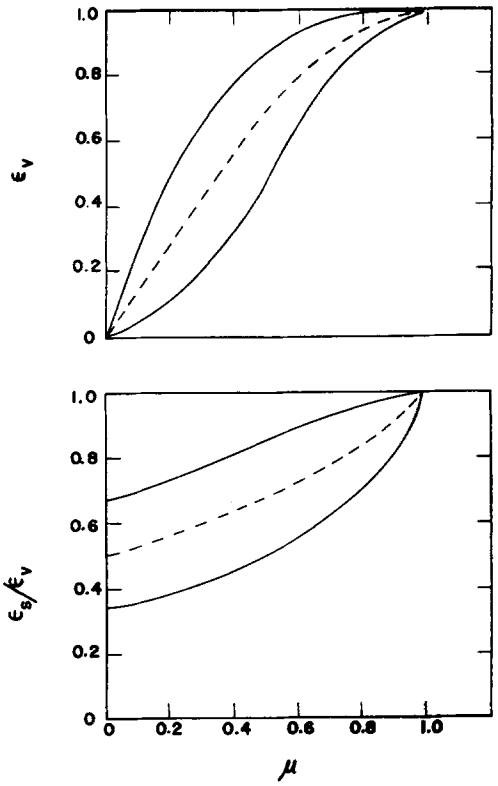

FIG. 3. Relationships between (ϵ_s/ϵ_v), ϵ_v and μ for block, Emmenthal, and combination structures. Upper solid line is block structure relationship and lower solid line is Emmenthal relationship for both cases. Dashed line represents linear combination of the results for the two structures.

The shape of the computed flux–pressure curve depends on the value of surface porosity used. The larger ϵ_s, the greater is the initial slope of this curve. Since the slopes of computed flux–pressure curves compare favorably with measured slopes,

as demonstrated in Figs. 5 to 8 of Part I, the value of surface porosity used is an acceptable value for the calculations. Assumption of an average value of $\epsilon_s = 0.6$

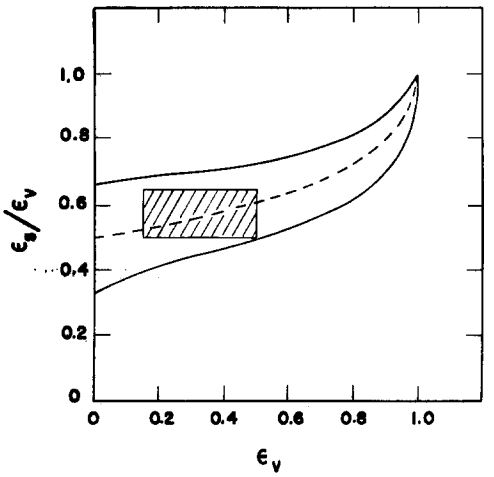

FIG. 4. Relationship between surface and volume porosity for block, Emmenthal, and combination structures. Upper solid line for block, lower solid line for Emmenthal, and dashed line for combination structure. Shaded area represents approximate practical range of porosities.

would result in even better fit of the data, though best results would be obtained by employing the (ϵ_s/ϵ_v) value corresponding to the values of Fig. 4 for each porous material studied. It is notable that according to this analysis the only instances where surface porosity is equal to volume porosity, as is often assumed, are in the trivial cases of ϵ_v of zero or unity.

EFFECT OF MIXING — DEFINITION OF THE MIXING EFFICIENCY

To this point the effect of mixing has been treated as an adjustable parameter employed to effect best fit of flux computation with experimental data. In Table 1 are the values of mixing efficiency employed for the fitting of experimental data; the results show that this quantity is a property of the solid and does not vary with pressure or temperature over the ranges studied. The mixing efficiency is not the same as the percent total pore length agreement used in previous work (*1*), but is uniquely related to it. We define mixing efficiency, η_E, as

$$\eta_E \equiv I_M/I_T \qquad (9)$$

where I_M is the number of available intersections in which mixing actually takes place and I_T is the total number of available intersections for the convergent–divergent array. Both values are determined by a simple counting procedure. The value of I_T is determined from the geometry of the array, as determined from the pore-size distribution, and computer calculation based on 100% length agreement (mixing between each minor pore segment). The values of I_M are determined for corresponding specific values of the percent length agreement by similar computation; a number of values for I_M so determined are used to establish the full range of mixing efficiencies as a function of length agreement. It has been found, at least in the present work, that the pore-

TABLE 1
MIXING EFFICIENCY RESULTS FOR POROUS MATERIALS

	Pellet				
	1	2	3	4	D[a]
Radius ($\bar{r}$, Å)	2800	340	355	380	600
Macropore porosity (ϵ_a)	0.27	0.15	0.20	0.28	0.39
Mixing efficiency (η_E)	0.01	1.00	0.88	0.77	0.66
Surface porosity (ϵ_s)	0.12	0.07	0.09	0.13	0.18
Mixing constant ($B \times 10^{-5}$)	1.55	1.11	1.17	1.24	1.12
Average for $B = (1.24 \times 10^5) \pm (0.18 \times 10^5)$					

[a] Reference (*2*).

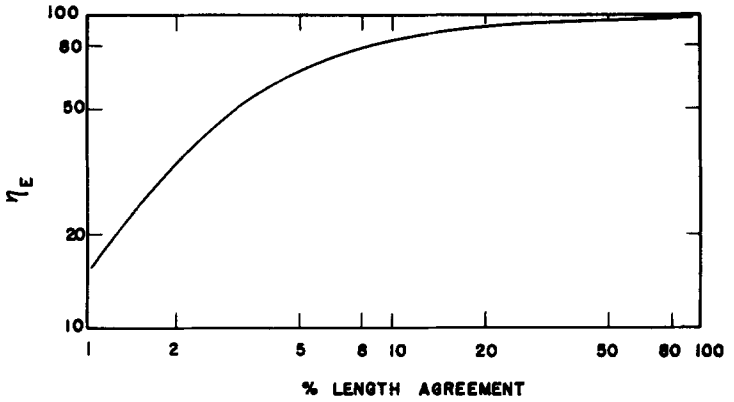

FIG. 5. Mixing efficiency as a function of percent length agreement for the porous structures of this study.

size distribution does not affect the functionality between mixing efficiency and length agreement parameter a great deal, thus a plot of η_E as a function of this parameter is given in Fig. 5 for all the porous materials studied.

CORRELATION OF THE MIXING EFFICIENCY WITH PROPERTIES OF THE POROUS STRUCTURE

The mixing efficiency of Eq. (9) has been found to correlate quite well with the most probable radius and the surface porosity of the materials employed. The empirical relationship established, wholly by trial with the data, is

$$(a/x)(\epsilon_s/\eta_E)^{1/2} = \text{constant} = B \quad (10)$$

Values of B determined for all the materials of this work, as well as for the previously correlated pellet of Wakao and Smith, are given in Table 1. These values are constant to within $\pm$ 14.5% which, in view of the range of porous structure properties involved, is quite good. The form of Eq. (10) can be justified by the following argument which gives a qualitative insight into the nature of the mixing process within porous structures. The basis of this development is that a similarity exists between the real structure of a porous material and that of the idealized block or Emmenthal structures insofar as mixing is concerned; the results are identical for the two, so the latter case is considered alone here. The similarity hypothesis is simply that the number of opportunities for a molecule traversing one pore to meet a molecule traversing another pore (that is, to mix) will be the same for a real structure and an Emmenthal structure of the same porosity, average radius, and other overall properties.

A rectangular plane, parallel to the direction of net axial transport, is considered in a porous pellet. In the real structure there will be by definition B_1^2 intersections between different pores in this plane; that is, there are B_1 intersections on a side. In the Emmenthal structure it was seen that there were n intersections on a side and hence n^2 intersections in any plane parallel to the direction of net axial transport. A molecule traversing the real structure in this plane would not enter into B_1^2 of these intersections, but would enter only a fraction of them so that only a fraction of the total opportunities to mix would be utilized. This is precisely the mixing efficiency definition of Eq. (9), thus actual mixing is $\eta_E B_1^2$ in the real structure. For the model structure the situation is analogous. Of the n^2 intersections available a molecule will enter into only some fraction of them, m, and the total number of mixes will be mn^2. Now by the similarity hypothesis

$$mn^2 = \eta_E B_1^2 \quad (11)$$

Let both m and B_1^2 be constant for any given situation, so that

$$(B_1^2/m) = \text{constant} = B^2 \quad (12)$$

From Eqs. (11) and (12)

$$B = n(1/\eta_E)^{1/2} \tag{13}$$

For the model structure, the surface porosity is related to n by

$$\epsilon_s = (nx/a)^2 \tag{14}$$

and

$$n = (a/x)(\epsilon_s)^{1/2} \tag{15}$$

Substituting the expression for n into Eq. (13) yields for B

$$B = (a/x)(\epsilon_s/\eta_E)^{1/2} \tag{10}$$

which is the form employed to correlate the experimental results. It is seen from the correlation of results that B is fairly constant for a wide range of structures, thus justifying *a posteriori* the statement of Eq. (12).

Conclusions

It is concluded that the proposed convergent–divergent pore model properly accounts for the measured fluxes, flux ratios, and their temperature and pressure dependence as measured in a Wicke-Kallenbach experiment. The correlation of results has been carried out for the argon-helium system and the four porous structures described here and for the nitrogen-helium system with alumina studied by Wakao and Smith. The computational model should permit the prediction of the effect of porous structure on the diffusional mass transport rate of any gas, in the absence of adsorption and surface migration, with only this input information: (1) the temperature, pressure, and molecular weights of the counterdiffusing pair, and (2) the pore volume–area distribution and the total porosity of the material. Such overall properties as most probable pore radius, surface porosity, and mixing efficiency are determined from the distribution and total porosity.

The computational parameters involved in the model, surface porosity, and mixing efficiency, are shown to be determinable from overall properties of the porous structure or from geometrical relationships pertaining to some limiting types of structure. Since mixing efficiency can be predicted, at least approximately, from surface porosity by Eq. (10), the convergent–divergent model can be used for predictive, as well as correlative, purposes. The correlation and interpretation of this study, based on the assumption that the micropores are all *culs-de-sac*, also leads to the conclusion that this portion of the pore volume–area distribution contributes very little to the overall transport effects of a porous material.

Acknowledgment

This work was supported by the National Science Foundation, by the Yale University Computer Center through a grant from the National Science Foundation, and by the donors of the Petroleum Research Fund, administered by the American Chemical Society.

References

1. Foster, R. N., and Butt, J. B., *AIChE J.* **11**, 180 (1966).
2. Wakao, N., and Smith, J. M., *Chem. Eng. Sci.* **17**, 825 (1962).
3. Le Goff, P., and Prost, C., *Genie Chimique* **95**, 1 (1966).